THE JOURNAL OF PHYSICAL CHEMISTRY B

Article

pubs.acs.org/JPCB

Green Synthesis of Reduced Graphene Oxide/Polyaniline Composite and Its Application for Salt Rejection by Polysulfone-Based Composite Membranes

Ilker Akin,[†] Erhan Zor,[‡,¶] Haluk Bingol,[*,§] and Mustafa Ersoz[†,⊥]

[†]Department of Chemistry, Faculty of Science, Selcuk University, Konya 42130, Turkey

[‡]Science Institute, Selcuk University, Konya 42130, Turkey

[¶]Science and Technology Department, A. K. Education Faculty, Necmettin Erbakan University, Konya 42090, Turkey

[§]Department of Chemistry, A. K. Education Faculty, Necmettin Erbakan University, Konya 42090, Turkey

[⊥]Advanced Technology R&D Center, Selcuk University, Konya 42130, Turkey

ABSTRACT: In this study, a novel, simple, and eco-friendly enzymatic-reaction-based approach to produce reduced graphene oxide/polyaniline (rGO/PANI) composite material was proposed. Glucose oxidase (GOx) was used as an effective catalyst producing hydrogen peroxide, in the presence of glucose, for the oxidative polymerization of aniline under ambient conditions. The prepared rGO/PANI composite was dispersed in polysulfone (PSf), and the mixed membranes were prepared by the phase inversion polymerization method. The morphology of membranes was investigated using scanning electron microscopy (SEM), atomic force microscopy (AFM), and contact angle (CA) techniques. The performance of membranes was studied in terms of salt rejection and pure water flux. The incorporation of rGO into the membrane matrix led to hydrophobic membrane surface with the enhanced macro-voids. On the contrary, the contact angle data revealed that the rGO/PANI-incorporated membrane surface is partly hydrophilic due to the PANI fibers in membrane, whereas SEM images showed the enhanced macro-voids. Membranes exhibited an improved salt rejection after rGO/PANI doping. The rGO/PANI-modified membrane loading exhibited a maximum of 82% NaCl rejection at an applied pressure of 10 bar. In addition, the results showed that the PSf-rGO/PANI composite membrane had the highest mean porosity and water flux.

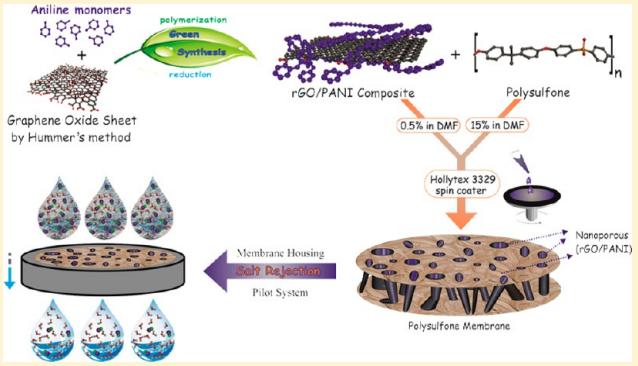

INTRODUCTION

In recent years, due to rapid population growth, global warming, and industrial development and thereby shortage, salination, and contamination of drinking water, the development of efficient water purification techniques has been an important global challenge facing humanity.[1,2] Desalination of seawater and brackish water has become one of the most promising approaches to produce fresh water from seas, oceans, and brackish reservoirs.[3−5] One of the most widely used purification techniques is membrane filtration due to its advantages such as high process flexibility, low energy requirement, and cost-effectiveness.[6,7] However, the development of commercial membranes has been significantly restricted due to membrane fouling which reduces water flux and permeate quality. In order to overcome these problems, the ideal membrane should provide thickness as thin as possible to maximize permeability. Furthermore, the ideal membrane should be mechanically robust to prevent fracture, chemically inert, and retain a high salt rejection rate, and it must possess a uniform pore distribution.[8]

Due to the fact that the flux across a membrane is inversely proportional to the thickness and pore size of the membrane, ultrathin and nanoporous membranes could greatly increase water permeability. Polymers, especially polysulfone (PSf), are prevalent and dominant membrane materials owing to their low cost, chemical compatibility, good heat resistance, easy processability, and resistance over a wide range of pH.[9] The main disadvantage of PSf membranes is their hydrophobic nature, whereas the desalination membranes require significant hydrophilicity in order to handle productivity problems. The most applied method for increasing the surface hydrophilicity is to mix the polymer matrix with some inorganic nanomaterials (TiO_2,[10] ZrO_2,[11] Al_2O_3, [12]and ZnO[13]) to produce composite membranes. The composite membranes were reported to show high antifouling performance due to the fact that these nanoparticles could enhance the membrane hydrophilicity.

Received: March 17, 2014
Revised: May 1, 2014
Published: May 9, 2014

Recent advances in nanotechnology have resulted in great achievements in the membrane technology for incorporation of carbon-based nanomaterials (such as carbon nanotube,[14] fullerene,[15] and graphene[16]) in order to produce thin and nanoporous membranes.[17,18] Graphene is a two-dimensional sheet of sp^2-hybridized carbon with the advantage of being the thinnest (one carbon diameter thick) material.[19] Recently, graphene and graphene oxide have gained much attention in the field of membrane research owing to its high surface area, chemical stability, and high mechanical strength. Application of graphene and its derivatives such as graphene oxide and functionalized graphene in the preparation of membranes can be examined from two directions.[20,21] The first is direct use of graphene as a separating layer,[22−24] and the second one is incorporating graphene and its derivatives in a polymer matrix for improving the membrane performance.[25,26]

Here we report another approach that may be applied by employing polymer-incorporated graphene composite materials to develop the complementary with the used polymer matrix (such as PSf). Polyaniline (PANI), a prototypical conjugated polymer, has been extensively studied by entrapment on graphene to enhance the performance of potential applications such as biosensors,[27] photocatalysts,[28] and supercapacitors.[29] Although carbon nanotube-templated PANI has been applied for membrane applications,[30] there is no study on the incorporation of graphene with polyaniline used as a membrane composite material. In this study, the successful fabrication of PSf-rGO/PANI composite membrane by mixing of the polymer (PSf) with the green synthesis product rGO/PANI was first reported. The membranes were prepared by the phase inversion polymerization method. The membrane structures and properties were characterized using atomic force microscopy (AFM), scanning electron microscopy (SEM), contact angle (CA), and porosity measurements. The pure water flux and salt rejection performance of membranes were investigated.

EXPERIMENTAL SECTION

Chemicals and Equipment. All chemicals were purchased from global suppliers and used without further purification. Graphite powder (99.99%), glucose oxidase (GOx) from *Aspergillus niger* (E.C.1.1.3.4.) 295 Umg^{-1}, D-(+)-glucose, aniline, PSf with M_w-35000, DMF, concentrated H_2SO_4 and H_3PO_4, H_2O_2 (30%), and $KMnO_4$ (99%) were purchased from Sigma-Aldrich Co., Germany. All aqueous solutions were freshly prepared using ultrapure water with a resistivity of 18.2 MΩ cm.

In order to characterize the GO, rGO, and rGO/PANI, Fourier transform infrared (FT-IR) and thermal gravimetric analysis (TGA) were used. Fourier transformed infrared (FT-IR) spectra of the samples were acquired between 550 and 4000 cm^{-1} wavenumber range using ATR FT-IR spectrometer (PerkinElmer 100 FT-IR). Thermogravimetric analysis (TGA) of the samples (10−15 mg) was performed on a Setaram thermal gravimetric analyzer (France) at temperature range of 20−1200 °C with 10°C min^{-1} heating ramp under argon atmosphere (gas flow rate: 20 mL min^{-1}).

In order to characterize the composite membranes, AFM, SEM, and CA measurements were used. AFM images were obtained from the tapping mode of a Park XE7 instrument. The speed of scanning was 1 Hz, and silicon nitride cantilevers were employed. The AFM images (of ca. 10 μm × 10 μm) of three different parts of each composite materials were analyzed to obtain the mean roughness parameter (R_a). The structures of composite samples were examined using a scanning electron microscope EVO-LS 10 (Carl Zeiss, Germany). Contact angle measurements were monitored by a horizontal beam comparator (KSV CAM 200). The contact angle measurements were taken as the mean value of three different points on each composite material. The sessile drop method was used to measure the contact angle of the prepared composite materials.[31,32] A 4 μL droplet of distilled water was placed on the samples surface by means of a 0.10 mL syringe, and the contact angle was measured by a horizontal beam comparator (KSV CAM 200). A magnified image of the droplet was recorded by a digital camera. Static contact angles were obtained from these images with calculation software.

Green Synthesis and Characterization of Reduced Graphene Oxide/Polyaniline Composite (rGO/PANI). Graphene oxide (GO) was prepared from graphite powder according to the improved method,[33] which has significant advantages over Hummer's method,[34] as indicated in the literature.[35,36] In order to obtain rGO/PANI, 20 mL of GO aqueous suspension (1 mg mL^{-1}) sonicated for 30 min was added into the GOx solution (1 mg mL^{-1}) in a round-bottom flask, and the solution was mixed for 30 min at 4 °C. Then, glucose (40 mM) and aniline (300 mM) were added into the solution (0.05 M A-PBS, pH 6.0) and mixed for 72 h. Finally, the product was filtered with a 0.2 μm, 25 mm cellulose membrane, washed with pure water (5 × 20 mL) and methanol (5 × 20 mL), and dried in vacuum oven at 50 °C.

The occurring polymerization of aniline on graphene sheets can be explained with four major substrates: aniline, monomer for polymerization; GOx, enzyme for generating hydrogen peroxide; glucose, reducing agent of graphene oxide (GO); dissolved oxygen, oxidizer for GOx. The reaction can be briefly explained as follows: Glucose reduces graphene oxide (eq 1).[37] GOx generates hydrogen peroxide and gluconolactone in the presence of dissolved oxygen and glucose (eq 2). It should be noted that the pH gradient locally decreases and H_2O_2 gradient increases because gluconic acid is formed in the solution (eq 3). Hence, the optimal conditions for the polymerization of aniline (eq 4) on rGO sheets are determined by locally formed H_2O_2 (eq 2) and locally decreased pH due to in enzymatic reaction formed gluconic acid (eq 3).[38,39]

$$\text{graphene oxide} \xrightarrow{\text{glucose}} \text{reduced graphene oxide} \quad (1)$$

$$\text{glucose} + O_2 \xrightarrow{\text{GOx}} \text{gluconolactone} + H_2O_2 \quad (2)$$

$$\text{gluconolactone} + H_2O \rightarrow \text{gluconic acid} \quad (3)$$

$$\text{aniline} + \text{rGO} \xrightarrow{\text{initiation by free radicals generated from } H_2O_2} \text{rGO/PANI composite} \quad (4)$$

Preparation and Characterization of PSf-rGO and PSf-rGO/PANI Flat Sheet Membranes. The composite membrane was prepared as depicted in the literature.[40,41] The polysulfone casting solution was prepared by dissolving the polymer (15%, w/w) in DMF by vigorous stirring for 12 h to get a homogeneous polymer solution. To this polymer solution, the desired amount (0.5%, w/w) of rGO and rGO/PANI distributed in DMF solvent was added. Then the solution was stirred for 24 h to obtain a uniform dispersion of rGO and rGO/PANI in casting solution. Spin coater (Laurell Model WS-400A-6NPP/LITE) was used for covering a polysulfone layer onto the nonwoven fabric support (Hollytex 3329). Then, the

dx.doi.org/10.1021/jp5025894 | J. Phys. Chem. B 2014, 118, 5707−5716

Scheme 1. Schematic Diagram for the Preparation of the PSf-rGO/PANI Composite Membrane

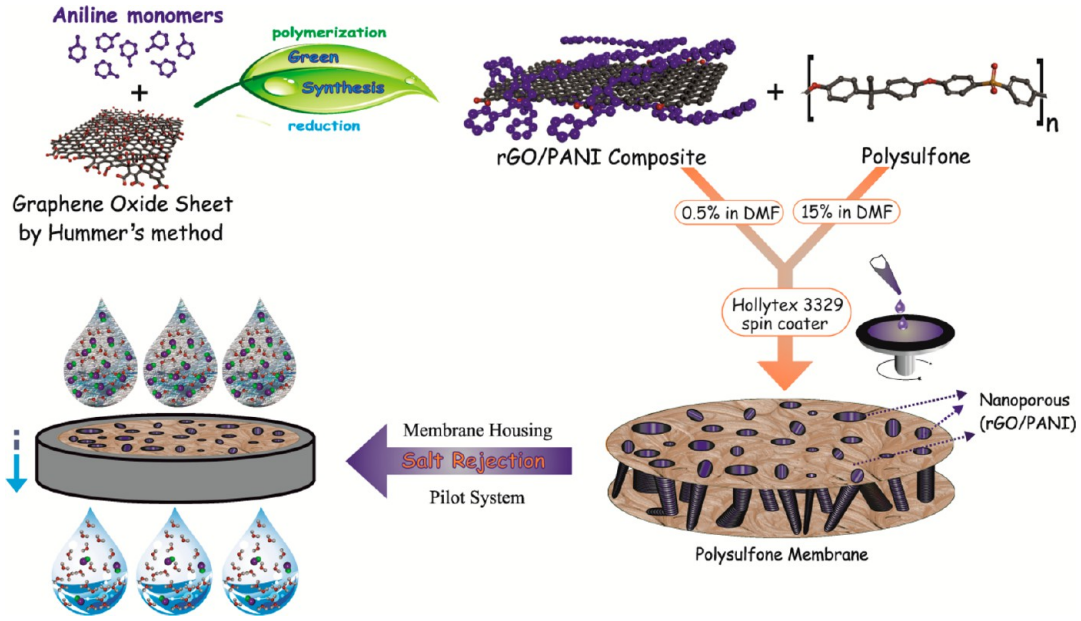

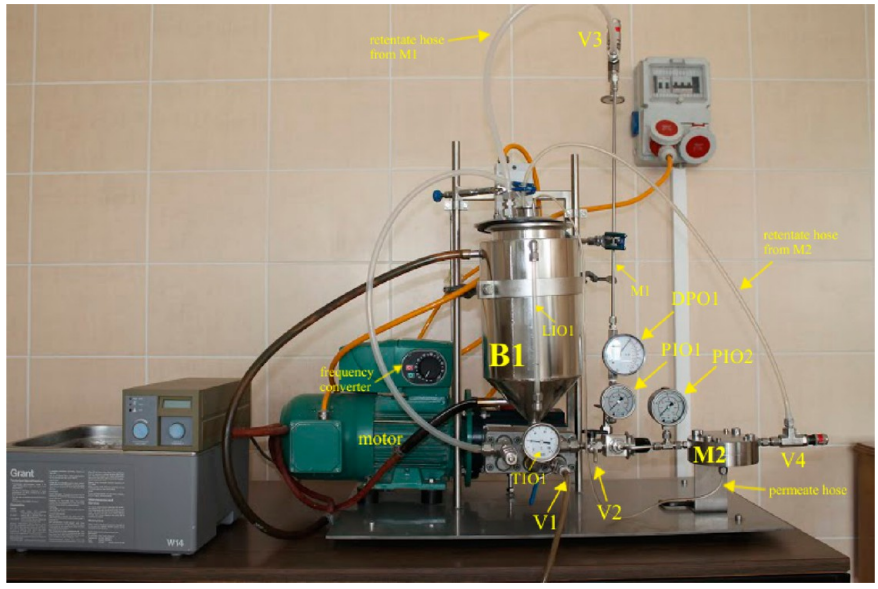

Figure 1. Flow diagram of the membrane plot plant. (M2: membrane housing; B1: feed tank with heating/cooling jacket; V1 and V2: emptying valve; V3: pressure regulation valve; V4: spring loaded valve; PI01 and PI02: pressure gage; DP01: differential pressure indicator; LI01: level indicator on the feed tank; TI01: temperature indicator.)

impregnated support was dipped in a water bath for 5 min at room temperature to induce phase inversion polymerization. The schematic representation for the preparation of the composite membrane is given in Scheme 1.

Pilot Plant and Performance Study of the Membranes. Flow diagram for the pilot plant (Prozesstechnick GmbH) is represented in Figure 1. The pilot plant includes a diaphragm pump controlled with a frequency converter (flow range: 1.8−12 L min^{-1}; pressure range: max 40 bar), feed tank with heating/cooling jacket (5 L capacity), and membrane housing for flat-sheet membranes.

The membrane performance was investigated by checking its pure water flux in order to determine the water transport behavior of the membrane. Then, the membranes were applied to salt rejection study using 1000 mg L^{-1} NaCl solutions. The effect of pressure on salt rejection and flux was also studied. The membranes having 44 cm^2 exposed area with a flat-sheet configuration were studied. The rejection of salt was calculated according to eq 5.

$$\text{salt rejection } (\%) = [1 - (C_p/C_f)]100 \quad (5)$$

where C_p and C_f are concentration of permeate and feed solution, respectively.

Porosity and Pore Size. The overall porosity (ε) was determined using gravimetric method, as defined in the following equation.[42]

$$\varepsilon = (\omega_1 - \omega_2)/Ald_w \quad (6)$$

dx.doi.org/10.1021/jp5025894 | J. Phys. Chem. B 2014, 118, 5707−5716

where ω_1 is the weight of the wet membrane, ω_2 is the weight of the dry membrane, A is the membrane effective area (m^2), d_w is the water density (998 kg m^{-3}), and l is the membrane thickness (m). All tests were replicated three times, and the mean values were taken into account. In addition, in order to determine the membrane mean pore radius (r_m), the Guerout–Elford–Ferry equation (eq 7), which is based on pure water flux and porosity data, was used.[42,43]

$$r_m = \sqrt{[(2.9 - 1.75\varepsilon)8\eta lQ]/(\varepsilon A \Delta P)} \quad (7)$$

where η is the water viscosity (8.9×10^{-4} Pa s), Q the permeation rate ($m^3\ s^{-1}$), and ΔP is the operational pressure (1 MPa).

RESULTS AND DISCUSSION

Characterization of rGO/PANI Composite. FTIR spectral analysis was performed to evaluate the reduction of oxygen-containing groups in GO by treating with glucose and to confirm the formation of rGO/PANI composite. Figure 2a shows the FTIR spectra of GO as well as the reduced samples, rGO and rGO/PANI, by the green method as depicted in the Experimental Section. The spectra have a broad band at around 3273 cm^{-1} for the O–H stretching vibration and a band at 1633 cm^{-1} for aromatic C=C stretching vibrations.[44,45] The spectrum of GO shows carbonyl C=O (1731 cm^{-1}), epoxy C–O (1221 cm^{-1}), and alkoxy C–O (1059 cm^{-1}) stretching vibrational modes.[45,46] After the reduction with glucose, the peak intensity at 1731 cm^{-1} described above greatly disappeared for the rGO and rGO/PANI composite. Also, the peak at 1221 and 1059 cm^{-1} and the broad band peak around 3273 cm^{-1} were weakened, indicating that most of the oxygen-containing functional groups of GO were removed after reduction.[47] These observations confirm that GO was successfully reduced to rGO using glucose as a reducing agent. Also, in the spectrum of rGO/PANI, the characteristic bands at 1297 and 1238 cm^{-1} are related to the C–N and C=N stretching modes, respectively, whereas the band at 1498 cm^{-1} can be attributed to C=C stretching vibration benzenoid rings in PANI.[48,49] The presence of these bands shows the successful coating of PANI on rGO sheets.

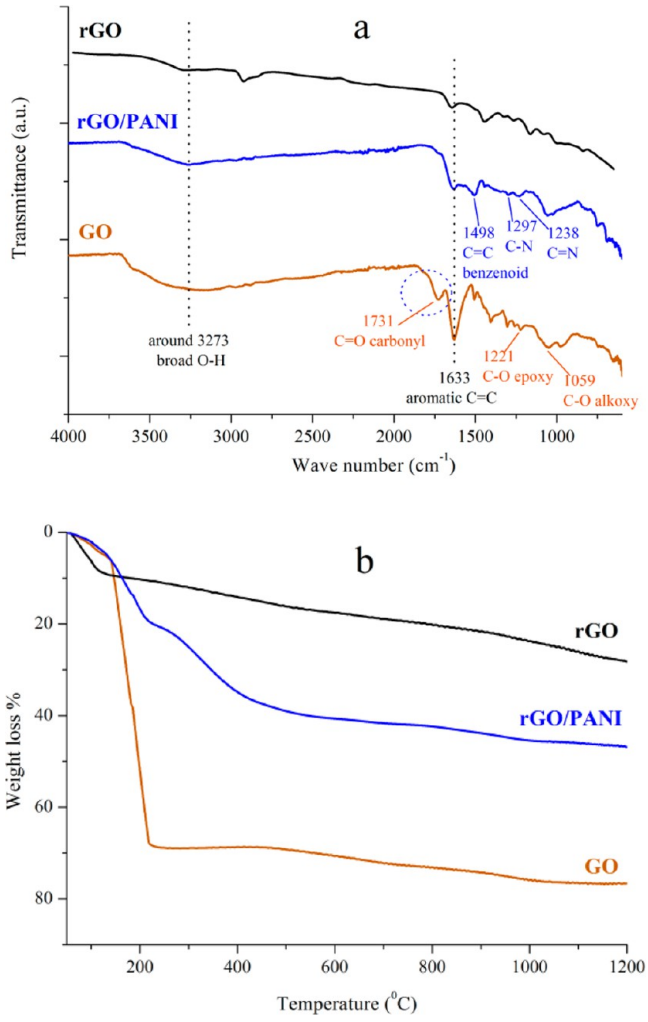

Figure 2. FTIR spectra (a) and TGA analysis curves (b) of GO, rGO, and rGO/PANI.

The thermal stability and the composition of GO, rGO, and rGO/PANI composite material were analyzed by TGA as can be seen in Figure 2b. GO is thermally unstable and shows a weight loss (4.38 wt %) up to 150 °C that could be primarily due to evaporation of water molecules and acidic residues held in the samples. Besides, GO has two major characteristic mass losses; the first and highest mass loss (64.6 wt %) appeared between 150 and 220 °C can be attributed to the decomposition of some oxygen-containing functional groups such as –OH, –CO, and –COOH yielding carbon monoxide, carbon dioxide, and water vapor as similarly indicated in the earlier reports.[50,51] The second mass loss started at 530 °C involves the pyrolysis of the remaining oxygen-containing groups and the burning of ring carbon.[52] Compared to GO, rGO showed much higher thermal stability (total weight loss of 28.8 wt %) because of the better graphitization and deoxygenation of rGO with enhanced van der Waals forces between layers,[53,54] which indicates the oxygen-containing functional groups are largely eliminated during the reduction process by glucose. In the case of rGO/PANI, the initial weight loss (21.3%) region around 120 °C is mainly attributed to the loss of adsorbed water molecules from the structures, whereas the rapid loss (21.3%) in the latter region started at 238 °C is assigned to the oxidative degradation of the composite itself. PANI starts to decompose at a comparatively low temperature less than 150 °C and is oxidized at about 665 °C, which is clearly evident.[55] These results indicate that most of the oxygen-containing groups of GO sheet were removed during the enzymatic reduction process, and the resultant rGO was covered with PANI obtained by polymerization of aniline, as described in the Experimental Section.

Characterization of the Prepared Membranes. Contact angle measurement was performed to investigate the hydrophilicity of the fabricated PSf membrane, PSf-rGO, and PSf-rGO/PANI composite membrane surfaces.[56] Figure 3(a–c) shows the contact images for PSf membrane, PSf-rGO, and PSf-rGO/PANI composite membranes taken at room temperature. The water contact angles of the PSf, PSf-rGO, and PSf-rGO/PANI membranes were found to be 82 ± 1°, 102 ± 2°, and 72 ± 1°, respectively [n = 3]. The PSf-rGO membrane showed the highest water contact angle of 102°. This indicates that the surfaces of rGO-doped membranes are relatively more hydrophobic in nature. Due to the fact that a lower contact angle leads to a more hydrophilic membrane surface in nature, it can be concluded that the PSf-rGO/PANI composite membrane represents the highest hydrophilicity, which results

dx.doi.org/10.1021/jp5025894 | J. Phys. Chem. B 2014, 118, 5707–5716

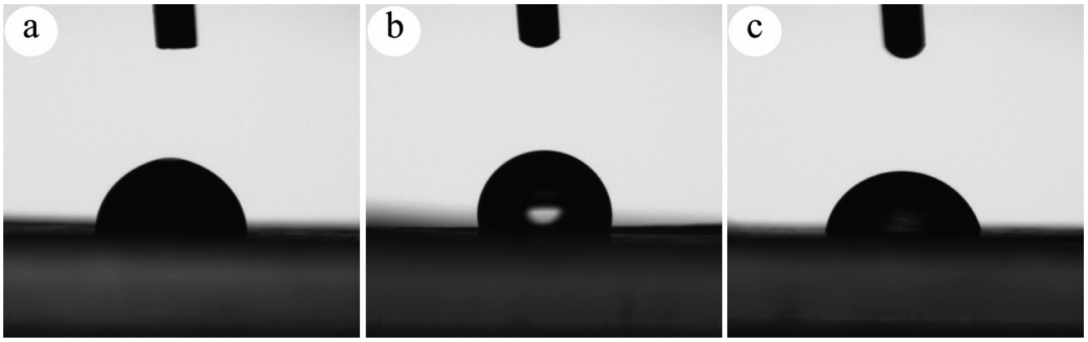

Figure 3. Drop images during contact angle measurements of (a) PSf membrane (b) PSf-rGO composite membrane, (c) PSf-rGO/PANI composite membrane.

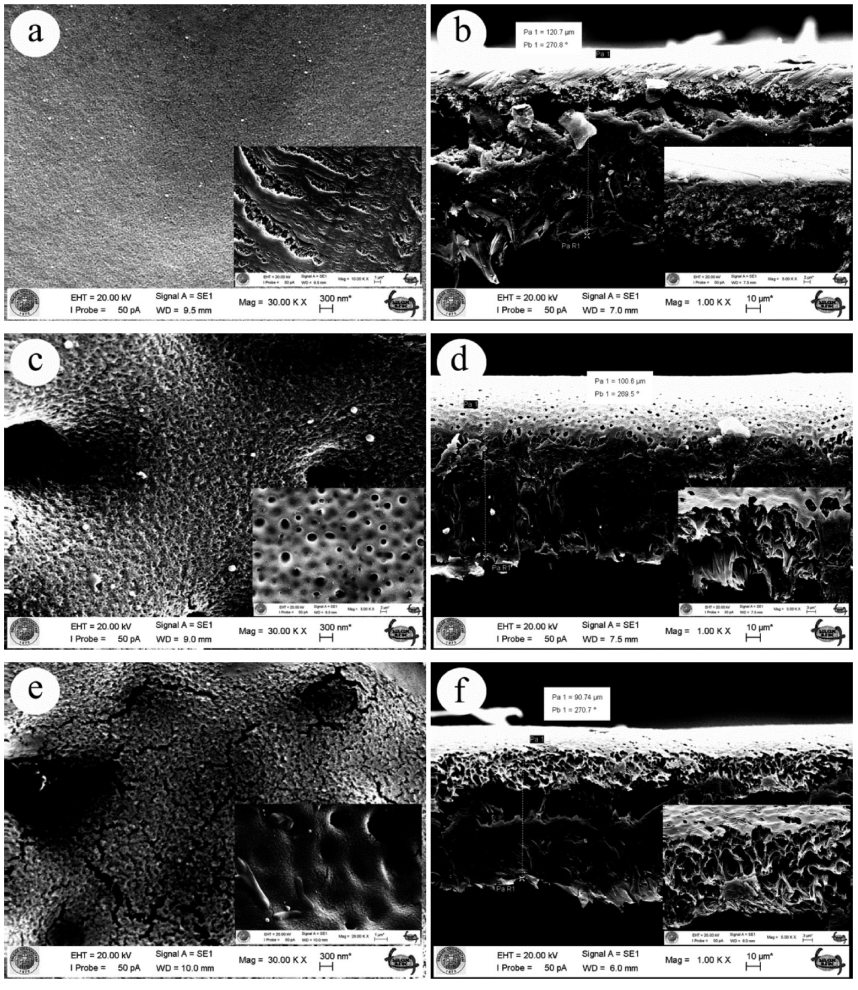

Figure 4. SEM images of the membranes. (a,b) PSf membrane surface and cross section, (c,d) PSf-rGO composite membrane surface and cross section, (e,f) PSf-rGO/PANI composite membrane and cross section.

in an increase in the water permeability of the membrane. Moreover, the addition of a hydrophilic component into the membrane casting solution resulted in acceleration of the exchange rate between solvent and nonsolvent, causing an increase in the pore size and hence the permeability of composite membranes. In other words, the increase of membrane hydrophilicity can be attributed to the spontaneously migration of hydrophilic nanoparticles and materials to the membrane/water interface to decrease the interface energy during the phase inversion polymerization.[57] The pore sizes of the prepared membranes were calculated according to Guerout–Elford–Ferry[42,43,58,59] equation, suggesting that the PSf-rGO/PANI composite membrane has the lowest pore size value of 4.2 nm.

Figure 4 represents the SEM images of blank PSf membrane, PSf-rGO, and PSf-rGO/PANI composite membrane surfaces and cross section, respectively. As shown in the blank PSf membrane (Figure 4a), the surface is smooth and a polymer lump or mass is not seen on the surface. As can be easily seen in Figure 4c, rGO caused the crater-like porous structure on the membrane surface. Also, the membrane surface is flat, and rGO clumping or mass is not seen, despite the fact that roughness

dx.doi.org/10.1021/jp5025894 | J. Phys. Chem. B 2014, 118, 5707–5716

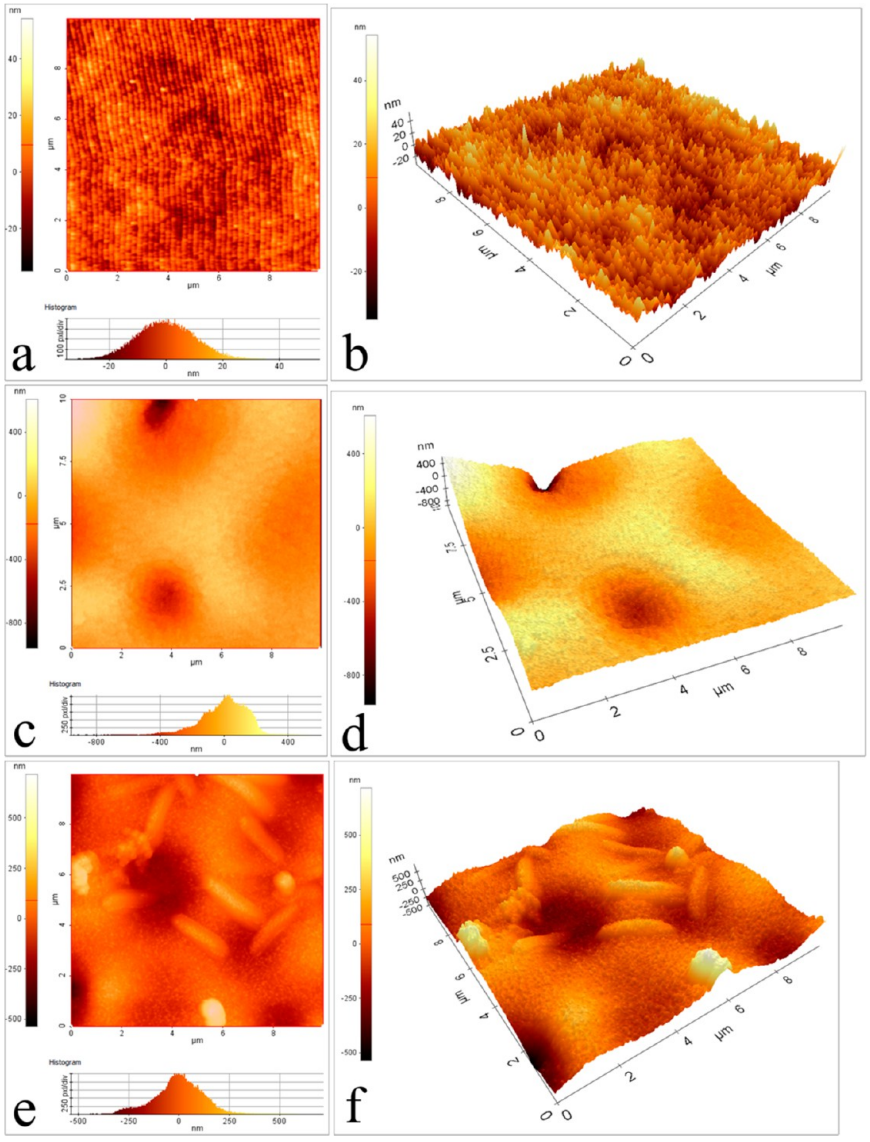

Figure 5. AFM images of the membranes. (a,b) PSf membrane 2D and 3D images, (c,d) PSf-rGO composite membrane 2D and 3D images, (e,f) PSf-rGO/PANI composite membrane 2D and 3D images.

increases on the surface. However, this mass and clumping are seen in noncarbonic-based nanoparticles.[20] In many noncarbonic nanoparticles such as TiO_2,[60] silica,[61] ZnO,[62] PANI/Fe_3O_4,[63] and Al_2O_3,[64] prepared by the phase inversion polymerization, the nanoparticles were obviously observed in the membrane surface. Nevertheless, in the case of the carbon-based nanofiller such as the carbon nanotube,[65,66] accumulation of CNTs was not observed. In the present results, it was observed at the membrane surface that rGO is homogeneously distributed in the polymer mixture. The macro-void structure was significantly altered by the addition of rGO/PANI to the polymer matrix (Figure 4c). This can be explained by the hydrophilic nature of rGO/PANI, which is responsible for the fast exchange of solvent and nonsolvent during the phase inversion polymerization, leading to expanded porosity as well as changes in the macro-void structure. Also, rGO/PANI accumulation around the membrane pores is observed in Figure 4e. rGO/PANI layer cracks in Figure 4e might result from the distortion during the preparation of SEM samples. The cross-sectional SEM images of the prepared blank (PSf membrane), PSf-rGO, and PSf-rGO/PANI composite membranes are exhibited in Figure 4b,d,f, respectively. We can observe that rGO/PANI causes the creation of the largest macro-voids in the rGO/PANI membrane (see Figure 4f). The addition of composite materials leads to growing and more apparent macro-voids. Therefore, the membrane having a more hydrophilic structure with the composite material can absorb and save much more water into the macro-voids, leading to a superior water content of the composite membrane. The cracks formed on the surface are clearly visible. In addition, it was observed that the membranes did not become fragile by the addition of rGO/PANI and that they have good stability.

Figure 5 represents the 2D−3D AFM images of the surface properties of blank (PSf membrane), PSf-rGO, and PSf-rGO/PANI composite membranes. These images showed that the membrane surfaces were not smooth. The PSf membrane (Figure 5a,b) displayed a relatively smooth surface and lesser aggregate formation compared to the PSf-rGO (Figure 5c,d) and PSf-rGO/PANI (Figure 5e,f) composite membranes. The mean roughness parameter R_a obtained from the AFM images

dx.doi.org/10.1021/jp5025894 | J. Phys. Chem. B 2014, 118, 5707−5716

showed values of 3.28, 69.37, and 53.37 nm for the PSf, PSf-rGO, and PSf-rGO/PANI membranes, respectively. Due to the fact that the membrane with lower roughness has stronger antifouling ability,[67] it can be understood from the roughness (R_a) parameter that the rGO (hydrophobic character) loading and also the surface roughness increased. On the other hand, the addition of hydrophilic character of rGO-PANI leads to a reduction in the R_a value. The PSf-rGO/PANI composite membrane has a lower roughness value than the PSf-rGO composite membrane, and this shows stronger antifouling ability of the PSf-rGO/PANI composite membrane. This may be caused by the fast exchange of solvent and nonsolvent occurring during the phase inversion polymerization because of the hydrophilic nature of PANI. As shown in Figure 5f, the fast exchange of solvents may result in the formation of lumps or nodules of polymer. As a result, the membrane surface would be rougher, and it may also increase the porosity as well.

Pure Water Flux and Salt Rejection of the Membranes. In order to study the influence of rGO and rGO/PANI loading on the membrane performance, the composite membranes containing rGO and rGO/PANI were prepared. The plots of pure water flux and salt rejection of PSf-rGO and PSf-rGO/PANI composite membranes are shown in Figure 6a.

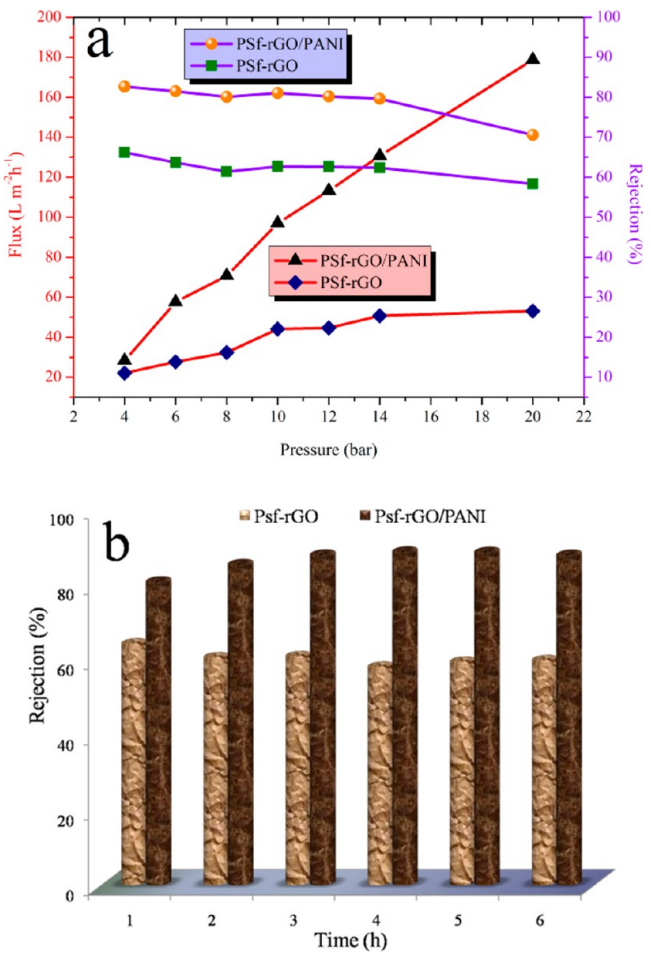

Figure 6. Effect of pressure on the pure water flux and rejection to NaCl of PSf-rGO and PSf-rGO/PANI composite membranes (red line: flux; blue line: rejection) (a), and effect of time on the rejection to NaCl of PSf-rGO and PSf-rGO/PANI composite membranes at 1 MPa operation pressure (b).

The PSf-rGO composite membrane exhibited low water flux due to its hydrophobic character as described above. Addition of rGO/PANI into the membrane matrix resulted in a more hydrophilic region facilitating the sorption of water into the membrane. As explained earlier for the SEM images, the same explanation can be justified by the water flux character of the membrane. Wu et al. stated that the addition of SiO_2−GO can improve the hydrophilicity of the membrane, promote the interaction between the membrane and the water molecules, and correspondingly help the water transport rate.[68] This situation was also observed by the addition of rGO/PANI. The pure water flux of the membrane significantly increased along with the rGO/PANI in the membrane. Also, it was observed that the formation of macro-voids increased during the phase inversion polymerization due to rGO/PANI doping. These increased macro-voids are also responsible for the observed increase in water flux. The prepared membranes were also examined for salt rejection studies. Salt rejection was carried out by checking the rejection of 1000 ppm of NaCl solutions at different applied pressure. The salt rejection showed that the PSf-rGO/PANI composite membrane is greater than the PSf-rGO composite membrane. The membrane with 0.5% (w/w) rGO/PANI loading showed the maximum salt rejection of 82% for NaCl at 10 bar pressure. The rejection exhibited a slightly decreasing trend with an increase of the pressure applied. At the same time, the NaCl rejection rates of membranes decreased vaguely with an increase of operating time (Figure 6b). However, it was observed that the decrease in rejection was not significant.

Porosity and Pore Size. The porosity of the prepared PSf, PSf-rGO, and PSf-rGO/PANI membranes was depicted in Figure 7. The hydrophilicity effect of rGO/PANI can increase

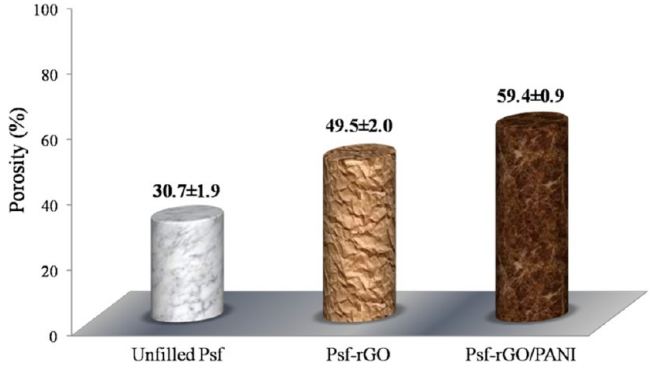

Figure 7. Porosity of the PSf, PSf-rGO, and PSf-rGO/PANI composite membranes.

the solvent and nonsolvent exchange during the phase inversion polymerization. This can lead to a higher porosity in the membrane surface (Figure 7) and improve the water permeability. The obtained results showed that the increase in porosity is different from the added the hydrophilic character of the rGO-based materials. Vatanpour et al.[42] reported a similar behavior for TiO_2 coated multiwalled carbon nanotubes embedding PES membranes. Also, the excess of the hydrophilic groups was found to increase porosity. As shown in the effect of pressure measurements above, the permeability of the PSf-rGO/PANI composite membrane increases continuously, but PSf-rGO composite membrane first increases slightly and then remains almost constant. The increase of porosity and hydrophilicity of the membrane with rGO/PANI content can

dx.doi.org/10.1021/jp5025894 | J. Phys. Chem. B 2014, 118, 5707−5716

attract water molecules into the membrane matrix. In addition, it facilitates their passage through the membrane and enhances the permeability. The pore sizes of membranes were calculated using the Guerout−Elford−Ferry equation given as eq 7. The mean pore radius values were found as 15.13, 8.7, and 4.22 nm for the PSf, PSf-rGO, and PSf-rGO/PANI membranes, respectively. The results indicate that composite membranes have a smaller mean pore size compared to pure PSf membranes because the mean pore radius decreases with the addition of rGO and rGO/PANI. These results demonstrate that adding appropriate rGO-based materials to PSf solution can improve its porosity and increase the small pore numbers, in accordance with similar results found in the literature.[69] As a result, the flux increased significantly with the addition of rGO/PANI.

CONCLUSION

In this paper, green synthesis of rGO/PANi composite produced by the enzymatic method was first reported. The rGO-based polymeric composite membranes were fabricated by the phase inversion polymerization method within polysulfone (PSf) polymer matrix through solution casting. The rGO/PANI composite exhibited suitable compatibility with polymeric components, which resulted in low agglomeration. Also, the rGO and rGO/PANI influenced surface mean pore size and porosity of the prepared composite membranes. The PSf-rGO/PANI composite membrane showed that the pure water flux is higher than the bare PSf membrane due to an increase of membrane hydrophilicity. The experiments showed that the rGO/PANI was a good modifier for salt rejection. This method for production of rGO/PANI composite allows for a high output of good surface mean pore size and porosity and most importantly membrane hydrophilicity. Also, this simple, rapid, and especially nontoxic enzymatic synthesis approach is expected to be a promising platform for incorporation of graphene sheets to the other polymers for the synthesis of novel graphene/polymer composites and production of graphene-based composite membranes using different enzymes and polymerizable monomers.

AUTHOR INFORMATION

Corresponding Author

*E-mail: halukbingol@gmail.com. Fax: +903323238225. Tel.: +903323238220−5499.

Notes

The authors declare no competing financial interest.

ACKNOWLEDGMENTS

The authors are grateful to the Scientific Research Projects of Necmettin Erbakan University (141710001) and Selcuk University (12101026) for financial support.

REFERENCES

(1) Ma, H.; Burger, C.; Hsiao, B. S.; Chu, B. Nanofibrous Microfiltration Membrane Based on Cellulose Nanowhiskers. *Biomacromolecules* **2012**, *13*, 180−186.

(2) Gao, P.; Sun, D. D.; Ng, W. J. Multifunctional Nanostructured Membrane for Clean Water Reclamation from Wastewater with Various pH Conditions. *RSC Adv.* **2013**, *3*, 15202−15210.

(3) Lin, S.; Buehler, M. J. Mechanics and molecular Filtration Performance of Graphyne Nanoweb Membranes for Selective Water Purification. *Nanoscale* **2013**, *5*, 11801−11807.

(4) Cohen-Tanugi, D.; McGovern, R. K.; Dave, S. H.; Lienhard, J. H.; Grossman, J. C. Quantifying the Potential of Ultra-permeable Membranes for Water Desalination. *Energy Environ. Sci.* **2014**, *7*, 1134−1141.

(5) Diban, N.; Aguayo, A. T.; Bilbao, J.; Urtiaga, A.; Ortiz, I. Membrane Reactors for In-Situ Water Removal: A Review of Applications. *Ind. Eng. Chem. Res.* **2013**, *52*, 10342−10354.

(6) Wang, P.; Ma, J.; Wang, Z.; Shi, F.; Liu, Q. Enhanced Separation Performance of PVDF/PVP- -MMT Nanocomposite Ultrafiltration Membrane Based on the NVP-Grafted Polymerization Modification of Montmorillonite (MMT). *Langmuir* **2012**, *28*, 4776−4786.

(7) Sun, A. C.; Kosar, W.; Zhang, Y.; Feng, V. Vacuum Membrane Distillation for Desalination of Water Using Hollow Fiber Membranes. *J. Membr. Sci.* **2014**, *455*, 131−142.

(8) Kou, J.; Zhou, X.; Lu, H.; Wu, F.; Fan, J. Graphyne as the Membrane for Water Desalination. *Nanoscale* **2014**, *6*, 1865−1870.

(9) Ganesh, B. M.; Isloor, A. M.; Ismail, A. F. Enhanced Hydrophilicity and Salt Rejection Study of Graphene Oxide-Polysulfone Mixed Matrix Membrane. *Desalination* **2013**, *313*, 199−200.

(10) Pan, J.; Zhang, X.; Du, A. J.; Sun, D. D.; Leckie, J. O. Self-Etching Reconstruction of Hierarchically Mesoporous F-TiO_2 Hollow Microspherical Photocatalyst for Concurrent Membrane Water Purifications. *J. Am. Chem. Soc.* **2008**, *130*, 11256−11257.

(11) Pang, R.; Li, X.; Li, J.; Lu, Z.; Sun, X.; Wang, L. Preparation and Characterization of ZrO_2/PES Hybrid Ultrafiltration Membrane with Uniform ZrO_2 Nanoparticles. *Desalination* **2014**, *332*, 60−66.

(12) Yan, L.; Li, Y. S.; Xiang, C. B. Preparation of Poly(vinylidene fluoride) (PVDF) Ultrafiltration Membrane Modified by Nano-Sized Alumina (Al_2O_3) and Its Antifouling Rresearch. *Polymer* **2005**, *46*, 7701−7706.

(13) Shen, L.; Bian, X.; Lu, X.; Shi, L.; Liu, Z.; Chen, L.; Hou, Z.; Fan, K. Preparation and Characterization of ZnO/Polyethersulfone (PES) Hybrid Membranes. *Desalination* **2012**, *293*, 21−29.

(14) Duan, W.; Dudchenko, A.; Mende, E.; Flyer, C.; Zhu X.; Jassby, D. Electrochemical Mineral Scale Prevention and Removal on Electrically Conducting Carbon Nanotube-Polyamide Reverse Osmosis Membranes. *Environ. Sci.: Processes Impacts*. In Press, DOI: 10.1039/c3em00635b.

(15) Tasaki, K.; Gasa, J.; Wang, H.; DeSousa, R. Fabrication and Characterization of Fullerene-Nafion Composite Membranes. *Polymer* **2007**, *48*, 4438−4448.

(16) Gai, J.-G.; Gong, X.-L.; Wang, W. W.; Zhang, X.; Kang, W.-L. An Ultrafast Water Transport Forward Osmosis Membrane: Porous Graphene. *J. Mater. Chem. A* **2014**, *2*, 4023−4028.

(17) Ellerie, J. R.; Apul, O. G.; Karanfil, T.; Ladner, D. A. Comparing Graphene, Carbon Nanotubes, and Superfine Powdered Activated Carbon as Adsorptive Coating Materials for Microfiltration Membranes. *J. Hazard. Mater.* **2013**, *261*, 91−98.

(18) Das, R.; Ali, M. E.; Hamid, S. B. A.; Ramakrishna, S.; Chowdhury, Z. A. Carbon Nanotube Membranes for Water Purification: A Bright Future in Water Desalination. *Desalination* **2014**, *336*, 97−109.

(19) Novoselov, K. S.; Geim, A. K.; Morozov, S. V.; Jiang, D.; Zhang, Y.; Dubonos, S. V.; Grigorieva, I. V.; Firsov, A. A. Electric Field Effect in Atomically Thin Carbon Films. *Science* **2004**, *306*, 666−669.

(20) Zinadini, S.; Zinatizadeh, A. A.; Rahimi, M.; Vatanpour, V.; Zangeneh, H. Preparation of A Novel Antifouling Mixed Matrix PES Membrane by Embedding Graphene Oxide Nanoplates. *J. Membr. Sci.* **2014**, *453*, 292−301.

(21) Jin, F.; Lv, W.; Zhang, C.; Li, Z.; Su, R.; Qi, W.; Yang, Q.-H.; He, Z. High-Performance Ultrafiltration Membranes Based on Polyethersulfone−Graphene Oxide Composites. *RSC Adv.* **2013**, *3*, 21394−21397.

(22) Sint, K.; Wang, B.; Kral, P. Selective Ion Pass Age Through Functionalized Graphene Nanopores. *J. Am. Chem. Soc.* **2008**, *130*, 16448−16449.

(23) Han, Y.; Xu, Z.; Gao, C. Ultra Thin Graphene Nano Filtration Membrane for Water Purification. *Adv. Funct. Mater.* **2013**, *23*, 3693−3700.
(24) Sun, P.; Zhu, M.; Wang, K.; Zhong, M.; Wei, J.; Wu, D.; Xu, Z.; Zhu, H. Selective Ion Penetration of Graphene Oxide Membranes. *ACS Nano* **2013**, *7*, 428−437.
(25) Heo, Y.; Im, H.; Kim, J. The Effect of Sulfonated Graphene Oxide on Sulfonated Poly (Etheretherketone) Membrane for Direct Methanol Fuel Cells. *J. Membr. Sci.* **2013**, *425−426*, 11−22.
(26) Zhao, Y.; Xu, Z.; Shan, M.; Min, C.; Zhou, B.; Li, Y.; Li, B.; Liu, L.; Qian, X. Effect of Graphite Oxide and Multi-Walled Carbon Nano Tubes on the Micro Structure and Performance of PVDF Membranes. *Sep. Purif. Technol.* **2013**, *103*, 78−83.
(27) Bo, Y.; Yang, H.; Hu, Y.; Yao, T.; Huang, S. A Novel Electrochemical DNA Biosensor Based on Graphene and Polyaniline Nanowires. *Electrochim. Acta* **2011**, *56*, 2676−2681.
(28) Ameen, S.; Seo, H.-K.; Akhtar, M. S.; Shin, H. S. Novel Graphene/polyaniline Nanocomposites and Its Photocatalytic Activity toward the Degradation of Rose Bengal Dye. *Chem. Eng. J.* **2012**, *210*, 220−228.
(29) Liu, H.; Wang, Y.; Gou, X.; Qi, T.; Yang, J.; Ding, Y. Three-Dimensional Graphene/Polyaniline Composite Material for High-Performance Supercapacitor Applications. *Mater. Sci. Eng., B* **2013**, *178*, 293−298.
(30) Liao, Y.; Yu, D.-G.; Wang, X.; Chain, W.; Li, X.-G.; Hoekde, E. M. V.; Kaner, R. B. Carbon Nanotube-Templated Polyaniline Nanofibers: Synthesis, Fash Welding and Ultrafiltration Membranes. *Nanoscale* **2013**, *5*, 3856−3862.
(31) Garbassi, F.; Morra, M.; Occhiello, E. *Polymer Surfaces From Physics to Technology*; Wiley: New York, 1994.
(32) Hwang, S.-T.; Kammermeyer, K. *Membranes in Separations, Techniques of Chemistry*; Wiley-Interscience: New York, 1975.
(33) Marcano, D. C.; Kosynkin, D. V.; Berlin, J. M.; Sinitskii, A.; Sun, Z.; Slesarev, A.; Alemany, L. B.; Lu, W.; Tour, J. M. Improved Synthesis of Graphene Oxide. *ACS Nano* **2010**, *4*, 4806−4814.
(34) Hummers, W. S.; Offeman, R. E. Preparation of Graphitic Oxide. *J. Am. Chem. Soc.* **1958**, *80*, 1339−1339.
(35) Zor, E.; Hatay Patir, I.; Bingol, H.; Ersoz, M. An Electrochemical Biosensor Based on Human Serum Albumin/Graphene Oxide/3-aminopropyltriethoxysilane Modified ITO Electrode for the Enantio-selective Discrimination of D- and L-tryptophan. *Biosens. Bioelectron.* **2013**, *42*, 321−325.
(36) Zor, E.; Saf, A. O.; Bingol, H.; Ersoz, M. Voltammetric Discrimination of Mandelic Acid Enantiomers. *Anal. Biochem.* **2014**, *449*, 83−89.
(37) Zhu, C.; Guo, S.; Fang, Y.; Dong, S. Reducing Sugar: New Functional Molecules for the Green Synthesis of Graphene Nano-sheets. *ACS Nano* **2010**, *4*, 2429−2437.
(38) Kausaite, A.; Ramanaviciene, A.; Ramanavicius, A. Polyaniline Synthesis Catalysed by Glucose Oxidase. *Polymer* **2009**, *50*, 1846−1851.
(39) Kausaite-Minkstimiene, A.; Mazeiko, V.; Ramanaviciene, A.; Ramanavicius, A. Enzymatically Synthesized Polyaniline Layer for Extension of Linear Detection Region of Amperometric Glucose Biosensor. *Biosens. Bioelectron.* **2010**, *26*, 790−797.
(40) Arslan, G.; Tor, A.; Muslu, H.; Ozmen, M.; Akin, I.; Cengeloglu, Y.; Ersoz, M. Facilitated Transport of Cr(VI) Through a Novel Activated Composite Membrane Containing Cyanex 923 as a Carrier. *J. Membr. Sci.* **2009**, *337*, 224−231.
(41) Paez-Hernandez, M. E.; Aguilar-Arteaga, K.; Valiente, M.; Ramirez-Silva, M. T.; Romero-Romo, M.; Palmomar-Pardave, M. Facilitated Transport of Hg(II) Through Novel Activated Composite Membranes. *Anal. Bioanal. Chem.* **2004**, *380*, 690−697.
(42) Vatanpour, V.; Madaeni, S. S.; Moradian, R.; Zinadini, S.; Astinchap, B. Novel Antibifouling Nanofiltration Polyethersulfone Membrane Fabricated from Embedding TiO_2 Coated Multi Walled Carbon Nanotubes. *Sep. Purif. Technol.* **2012**, *90*, 69−82.
(43) Hamid, N. A. A.; Ismail, A. F.; Matsuura, T.; Zularisam, A. W.; Lau, W. J.; Yuliwati, E.; Abdullah, M. S. Morphological and Separation Performance Study of Polysulfone/Titanium Dioxide (PSF/TiO_2) Ultrafiltration Membranes for Humic Acid Removal. *Desalination* **2011**, *273*, 85−92.
(44) Bao, C.; Guo, Y.; Yuan, B.; Hu, Y.; Song, L. Functionalized Graphene Oxide for Fire Safety Applications of Polymers: A Combination of Condensed Phase Flame Retardant Strategies. *J. Mater. Chem.* **2012**, *22*, 23057−23063.
(45) Travlou, N. A.; Kyzas, G. Z.; Lazaridis, N. K.; Deliyanni, E. A. Functionalization of Graphite Oxide with Magnetic Chitosan for the Preparation of a Nanocomposite Dye Adsorbent. *Langmuir* **2013**, *29*, 1657−1668.
(46) Feng, Y.; Feng, N.; Du, G. A Green Reduction of Graphene Oxide via Starch-Based Materials. *RSC Adv.* **2013**, *3*, 21466−21474.
(47) Chandra, V.; Kim, K. S. Highly Selective Adsorption of Hg^{2+} by a Polypyrrole−Reduced Graphene Oxide Composite. *Chem. Commun.* **2011**, *47*, 3942−3944.
(48) Zhang, J.; Zhao, X. S. Conducting Polymers Directly Coated on Reduced Graphene Oxide Sheets as High-Performance Supercapacitor Electrodes. *J. Phys. Chem. C* **2012**, *116*, 5420−5426.
(49) Zhang, K.; Zhang, L. L.; Zhao, X. S.; Wu, J. Graphene/Polyaniline Nanofiber Composites as Supercapacitor Electrodes. *Chem. Mater.* **2010**, *22*, 1392−1401.
(50) Feng, H.; Cheng, R.; Zhao, X.; Duan, X.; Li, J. A Low-Temperature Method to Produce Highly Reduced Graphene Oxide. *Nat. Commun.* **2013**, *4*, 1539−1546.
(51) Kumar, N. A.; Choi, H. J.; Shin, Y. R.; Chang, D. W.; Dai, Li.; Baek, J. B. Polyaniline-Grafted Reduced Graphene Oxide for Efficient Electrochemical Supercapacitors. *ACS Nano* **2012**, *6*, 1715−1723.
(52) Mao, S.; Pu, H.; Chen, J. Graphene Oxide and Its Reduction: Modeling and Experimental Progress. *RSC Adv.* **2012**, *2*, 2643−2662.
(53) Dikin, D. A.; Stankovich, S.; Zimney, E. J.; Piner, R. D.; Dommett, G. H. B.; Evmenenko, G.; Nguyen, S. T.; Ruoff, R. S. Preparation and Characterization of Graphene Oxide Paper. *Nature* **2007**, *448*, 457−460.
(54) Li, X.; Zhang, G.; Bai, X.; Sun, X.; Wang, X.; Wang, E.; Dai, H. Highly Conducting Graphene Sheets and Langmuir-Blodgett Films. *Nat. Nanotechnol.* **2008**, *3*, 538−542.
(55) Gheno, G.; de Souza Basso, N. R.; Hübler, R. Polyaniline/Graphite Nanocomposites: Synthesis and Characterization. *Macromol. Sym.* **2011**, *299−300*, 74−80.
(56) Wu, C. M.; Xu, T. W.; Yang, W. H. Fundamental Studies of a New Hybrid (Inorganic−Organic) Positively Charged Membrane: Membrane Preparation and Characterizations. *J. Membr. Sci.* **2003**, *216*, 269−278.
(57) Celik, E.; Liu, L.; Choi, H. Protein Fouling Behavior of Carbon Nanotube/Polyethersulfone Composite Membranes During Water Filtration. *Water Res.* **2011**, *45*, 5287−5294.
(58) Li, J. F.; Xu, Z. L.; Yang, H.; Feng, C. P.; Shi, J. H. Hydrophilic Microporous PES Membranes Prepared by PES/PEG/DMAc Casting Solutions. *J. Appl. Polym. Sci.* **2008**, *107*, 4100−4108.
(59) Chakrabarty, B.; Ghoshal, A. K.; Purkait, M. K. Effect of Molecular Weight of PEG on Membrane Morphology and Transport Properties. *J. Membr. Sci.* **2008**, *309*, 209−221.
(60) Vatanpour, V.; Madaeni, S. S.; Khataee, A. R.; Salehi, E.; Zinadini, S.; Monfared, H. A. TiO_2 Embedded Mixed Matrix PES Nano Composite Membranes: Influence of Different Size Sand Types of Nanoparticles on Antifouling and Performance. *Desalination* **2012**, *292*, 19−29.
(61) Wu, H.; Mansouri, J.; Chen, V. Silica Nanoparticles as Carriers of Antifouling Ligands for PVDF Ultrafiltration Membranes. *J. Membr. Sci.* **2013**, *433*, 135−151.
(62) Leo, C. P.; Lee, W. P. C.; Ahmad, A. L.; Mohammad, A. W. Polysulfone Membranes Blended with ZnO Nanoparticles for Reducing Fouling by Oleic Acid. *Sep. Purif. Technol.* **2012**, *89*, 51−56.
(63) Daraei, P.; Madaeni, S. S.; Ghaemi, N.; Salehi, E.; Khadivi, M. A.; Moradian, R.; Astinchap, B. Novel Polyethersulfone Nano Composite Membrane Prepared by $PANI/Fe_3O_4$ Nanoparticles with Enhanced Performance for Cu(II) Removal from Water. *J. Membr. Sci.* **2012**, *415*, 250−259.

(64) Jiansheng, L.; Lianjun, W.; Yanxia, H.; Xiaodong, L.; Xiuyun, S. Preparation and Characterization of Al_2O_3 Hollow Fiber Membranes. *J. Membr. Sci.* **2005**, *256*, 1−6.
(65) Vatanpour, V.; Madaeni, S. S.; Moradian, R.; Zinadini, S.; Astinchap, B. Fabrication and Characterization of Novel Antifouling Nanofiltration Membrane Prepared from Oxidized Multi Walled Carbon Nanotube/Polyethersulfone Nanocomposite. *J. Membr. Sci.* **2011**, *375*, 284−294.
(66) Choi, J.-H.; Jegal, J.; Kim, W. N. Fabrication and Vharacterization of Multi-Walled Carbon Nanotubes/Polymer Blend Membranes. *J. Membr. Sci.* **2006**, *284*, 406−415.
(67) Rana, D.; Matsuura, T. Surface Modifications for Antifouling Membranes. *Chem. Rev.* **2010**, *110*, 2448−2471.
(68) Wu, H.; Tang, B.; Wu, P. Development of Novel SiO_2−GO Nanohybrid/Polysulfone Membrane with Enhanced Performance. *J. Membr. Sci.* **2014**, *451*, 94−102.
(69) Yang, Y.; Zhang, H.; Wang, P.; Zheng, Q.; Li, J. The Influence of Nano-Sized TiO_2 Fillers on The Morphologies and Properties of PSF UF Membrane. *J. Membr. Sci.* **2007**, *288*, 231−238.